Local void fraction and heat transfer characteristics around tubes in two-phase flows across horizontal in-line and staggered tube bundles

Murakawa, Hideki ; Baba, Misaki ; Miyazaki, Takeru ; Sugimoto, Katsumi ; Asano, Hitoshi ; Ito, Daisuke

(Citation)
Nuclear Engineering and Design,334:66-74

(Issue Date)
2018-08-01

(Resource Type)
journal article

(Version)
Accepted Manuscript

(URL)
https://hdl.handle.net/20.500.14094/90004947

Local void fraction and heat transfer characteristics around tubes in two-phase flows across horizontal in-line and staggered tube bundles

Hideki Murakawa[1], Misaki Baba[1], Takeru Miyazaki[1], Katsumi Sugimoto[1], Hitoshi Asano[1], Daisuke Ito[2]

[1]Kobe University, 1-1 Rokkodai, Nada, Kobe 657-8501 Japan
[2] Research Reactor Institute, Kyoto University, 2 Asashiro-nishi, Kumatori, Sennan, Osaka 590-0494 Japan

Corresponding author: Hideki Murakawa, E-mail: murakawa@mech.kobe-u.ac.jp

Abstract

This study investigated the local characteristics of void-fraction distribution and heat transfer around tubes in two-phase flows under adiabatic conditions using vertical duct test sections with inner dimensions of 90 × 90 mm^2. Two kinds of test sections, in-line and staggered tube bundles, each containing five columns and eight rows, were employed for the measurements. The tube diameter of each was 15 mm, and the pitch-to-diameter ratio was 1.5 for both bundles. The working fluids were air and water, and the experiments were performed under atmospheric pressure in a temperature range of 20–25 ºC. Superficial liquid velocity, J_L, and gas velocity, J_G, ranged from 0.1 to 0.3 m/s and 0.03 to 1.19 m/s, respectively. Two-dimensional void-fraction distributions were obtained using X-ray radiography and the local heat-transfer coefficients were measured using a platinum wire electrode placed on a tube that could be rotated. In the experiments, the time-averaged void fraction increased at the maximum and vertical minimum gaps for the in-line tube bundle, whereas the void fraction increased upstream of the tubes for the staggered tube bundle. In the bubbly flow condition, enhancement of the heat transfer by bubbles motion clearly occurred between ±90 and 180° for the in-line tube bundle, and increased all over the pipe for the staggered tube bundle. The increase in the local heat transfer coefficients by bubbles motion was more apparent for the in-line tube bundle. The average heat transfer coefficient in the staggered tube bundle was higher than that in the in-line tube bundle in the bubbly flow regime, whereas the results were opposite in the intermittent flow regime.

Keywords:

Heat exchanger, Void fraction, Heat transfer coefficient, Flow regime

Highlights:

- ✓ Local void fraction and heat transfer coefficients were experimentally investigated.
- ✓ Void fractions and heat transfers for in-line and staggered arrays were compared.
- ✓ Agitation effects by bubbles motion change with the tube array and the flow regime.
- ✓ Local heat transfer coefficients increase with the void fraction.
- ✓ Increased heat transfer by bubbles motion was more apparent for in-line bundle.

1. Introduction

Knowledge of the two-phase flow characteristics across horizontal tube bundles in heat exchangers such as steam generators in pressurized water reactors, PWRs, and kettle reboilers is important. The void fraction and pressure drop in the flow channel are important parameters for predicting these flow characteristics, fluid oscillation, and heat transfer. Consequently, numerous experimental studies have been carried out in test loops with horizontal tube bundles to clarify two-phase flow phenomena.

Xu et al. (1998) compared the flow pattern, void fraction, and pressure drop in vertical upward and downward flows. Using an in-line tube arrangement and a pitch-to-diameter ratio, p/d, of 1.28, they showed the variation of void fraction with flow direction. Ulbrich and Mewes (1994) focused on flow regime clarification. They compared their experimental results with results associated with several tube geometries presented in the literature and proposed a new flow pattern map. Subsequently, they concluded that further investigations considering geometry factors such as pipe diameter and pitch were required.

Kondo and Nakajima (1980) investigated the spatial-average void fractions in staggered tube bundles with three different p/d conditions and proposed an empirical equation for predicting the mean void fraction containing the pitch effect. Dowlati et al. (1990, 1992) investigated the pressure drop and void fraction in in-line tube bundles with p/d 1.3 and 1.75 and showed that the two-phase pressure drop increased with p/d. They also investigated the pressure drop and the void fraction in staggered tube bundles, in which case they concluded that p/d had no effect on theses parameters. McNeil et al. (2012) investigated void fraction at minimum and maximum gaps between tubes in in-line bundle using the γ-ray, and compared the difference of the void fraction. They showed that the void fraction at the maximum gap is suitable to use for the drift flux model. For these experimental studies, the γ-ray density meter is a powerful tool for measuring void fraction although the spatial resolution for the measurement is limited.

Noghrehkarm et al. (1999) employed an electrical resistivity void probe to evaluate the local void fraction and further proposed a method to identify the flow regime based on the probability density function (PDF) of the signal. Aprin et al. (2007, 2011) used an optical fiber probe to obtain the local void fraction in a staggered tube bundle. However, many of these studies evaluated the local void fraction at several measurement positions in the tube bundles, and did not conduct sufficient two-

dimensional void-fraction distributions in the bundles. To observe the local liquid velocity fields and bubbles motion around the tubes for in-line and staggered arrays, particle image velocimetry (PIV) was utilized by Iwaki et al. (2005). They reported that the wake regions of tubes made the void fraction distributions in staggered bundles uniform. Furthermore, they evaluated average void fractions using image processing and showed that the void fraction in staggered bundles is slightly higher than that in the in-line tube bundle in bubbly flow at a void fraction of less than 0.03.

Chan and Shoukri (1987) investigated the heat-transfer coefficient in in-line array tubes under pool boiling. Their results indicated that the heat-transfer coefficients in the upper row tubes were higher than those in the lower row tubes. Consequently, they concluded that the heat-transfer process was strongly influenced by the two-phase convection effects under low-quality conditions. Dowlati et al. (1996) investigated the average boiling heat transfer in in-line array tubes and showed that the heat-transfer coefficient increases with the heat flux in the nucleate boiling region. Burnside et al. (2001) investigated the heat-transfer coefficient along the flow direction and showed that the coefficient decreased marginally as the bundle row increases. Karas et al. (2014) investigated the heat-transfer coefficient around a tube with the aid of an electrochemical technique that enabled them to obtain the local heat transfer around the tube. However, the relation between the local void fraction and the heat transfer around the tube was not fully investigated.

It is known that bubbles motion agitates the liquid phase, resulting in increased heat transfer in the nucleate boiling region of two-phase flows. Hence, clarification of the relation between bubbles motion and heat transfer is important for optimizing the heat exchanger. This study was conducted with the objective of clarifying the local characteristics of void-fraction distribution and heat transfer around tubes in two-phase flows under adiabatic conditions. In particular, focus was placed on the flow regime of bubbly and intermittent flows that mainly appear in the upstream region of the heat exchangers. In this study, two-dimensional void-fraction distributions were measured using X-ray radiography, and the heat-transfer coefficients around each tube obtained using a platinum wire placed on a measurement tube. Subsequently, the results obtained for in-line and staggered tube bundles at a pitch-to-diameter ratio of 1.5 were compared.

2. Experimental setup

2.1. Experimental loop and test sections

A schematic diagram of the experimental facility is shown in Fig. 1. The test section was a vertical duct with a cross-section of 90 × 90 mm^2. Water was circulated through a liquid injector located at the bottom of this test section. Further, air was injected into the test section through two porous tubes made of polypropylene (Spacy Chemical Ltd., P-200) with a mean pore-diameter of 200 μm and porosity of 38%. The porous tubes were located at its base in a direction perpendicular to the tube bundles. The air flow rates were measured in each porous tube using mass flow meters (HORIBA Ltd., MF-F). We employed two maximum flow rate ranges: 50 L/min and 200 L/min. The accuracy of the flowmeters was ±3% at full scale. The water flow rate was measured using a paddle wheel flowmeter (AICHI TOKEI, ND20) with an accuracy of ±2% in the reading scale. The two-phase mixture flowed upward through tube bundles set in the test section. The distance between the air injector and the bottom of the bundle was approximately 650 mm, and the top of the tube bundle was approximately 670 mm below the water surface in the overhead tank.

As shown in Fig. 2, two different tube bundles were employed for the measurements: (1) an in-line tube bundle with eight rows of three full tubes and two half tubes on the walls; (2) a staggered tube bundle with eight rows. The tubes were 90 mm long and the outer diameter, d, was 15 mm in both bundles. The tubes pitch, p, was 22.5 mm and the pitch-to-diameter ratio, p/d, was 1.5.

The experiments were performed at 20–25 ºC with varying superficial liquid velocity, J_L, from 0.1 to 0.3 m/s, corresponding to mass flux, G, from 100 to 300 kg/(m^2s) and superficial gas velocity, J_G, from 0.03 to 1.19 m/s under atmospheric pressure. The superficial velocities and the mass flux were defined at the minimum cross-sectional area, labelled “A” in Fig. 2.

A high-speed camera (FASTCAM SA 1.1, Photron Ltd.) with a frame rate 1,000 fps and shutter speed 1/2,000 was employed to observe the flow regimes in two-phase flow.

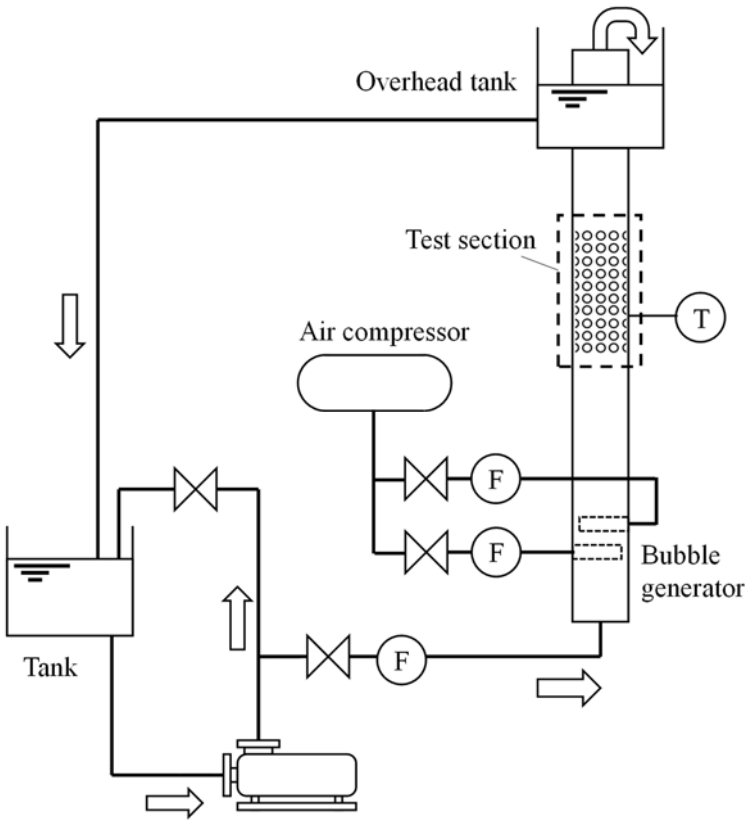

Fig. 1. Experimental test loop.

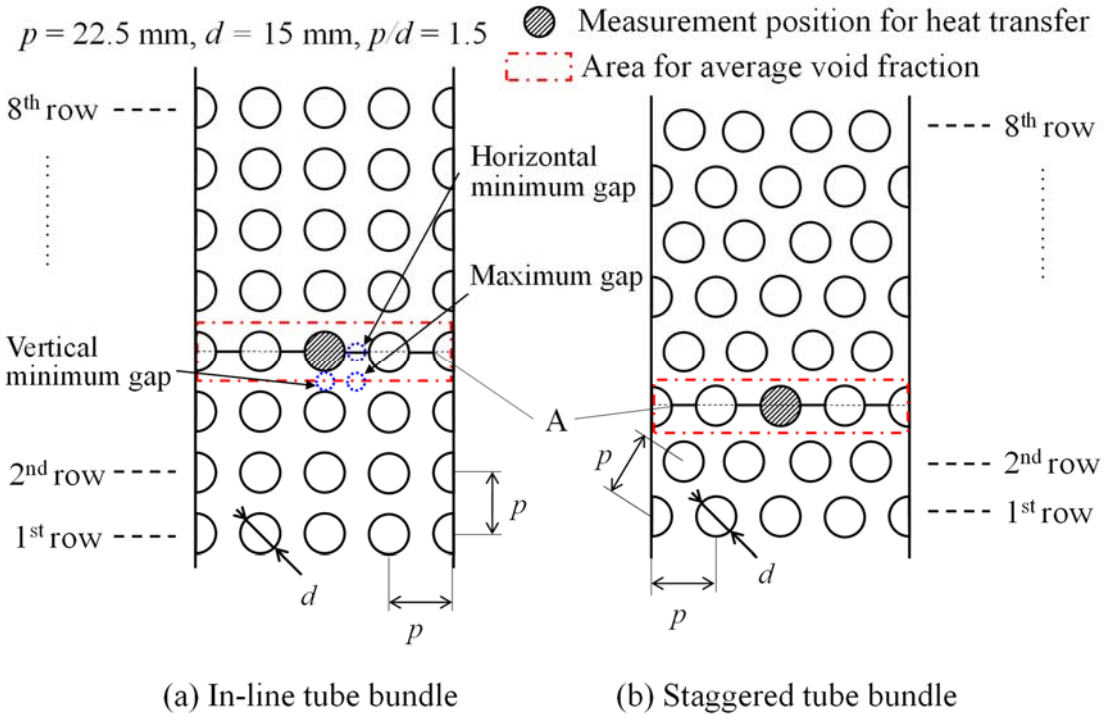

Fig. 2. Schematic of the test section bundles.

2.2. X-ray radiography

X-ray radiography is based on the difference in X-ray attenuation resulting from a material and its thickness. The X-ray attenuation caused by water is higher than that caused by air because of the difference in their densities. Two-dimensional void-fraction distributions can be calculated from the brightness distributions based on the characteristics of the X-ray attenuation in the medium. Thus, it is known that the void-fraction distribution is obtained by processing three images—gas-filled, liquid-field and two-phase mixture-filled. Assuming that the intensity of the X-ray is proportional to the brightness distribution on the *x*-*y* plane, $S(x, y)$ can be expressed as follows:

$$S_G(x,y) = A(x,y)\exp[-\rho_M \mu_{mM} t_M(x,y)] + O_G(x,y) \quad (1)$$

$$S_L(x,y) = A(x,y)\exp[-\rho_M \mu_{mM} t_M(x,y) - \rho_L \mu_{mL} t(x,y)] + O_L(x,y) \quad (2)$$

$$S_{TP}(x,y) = A(x,y)\exp[-\rho_M \mu_{mM} t_M(x,y) - \{1-\alpha(x,y)\}\rho_l \mu_{mL} t(x,y)] + O_{TP}(x,y) \quad (3)$$

where A is the gain, O is the offset, ρ is the density, μ_m is the mass attenuation coefficient and α is the average void fraction along the beam direction. The subscripts G, L, and TP signify gas, liquid, and two-phase mixture, respectively, and M represents the material of the test section. Thus, the two-dimensional void fraction of $\alpha(x, y)$ can be determined as follows:

$$\alpha(x,y) = \frac{\ln\left\{\dfrac{S_{TP}(x,y) - O_{TP}(x,y)}{S_L(x,y) - O_L(x,y)}\right\}}{\ln\left\{\dfrac{S_G(x,y) - O_G(x,y)}{S_L(x,y) - O_L(x,y)}\right\}} \quad (4)$$

To obtain the offset terms in the equation, lead chips were placed on the wall of the test section at the tube position.

Fig. 3 shows a schematic of the experimental X-ray radiography system. The X-ray enters from the side along the axial direction of the tubes and is attenuated by the two-phase mixtures. The transmitted X-ray is then converted to visible light using an image intensifier (I.I.), and 10-bit gray-scale radiographs are taken using a high-speed camera (MotionPro Y-4 Lite, IDT Inc.) with an array of 1024 × 1024 pixels, with pixel size 170 μm. In the experiments, the frame rate was set at 30 fps and 450 radiographs, which correspond to 15 s, were taken in each condition. Further, the X-ray was generated at 80 kV and 5 mA.

The parallelism of the X-ray beam is associated with image blurring and is defined by the

setting geometry of the measurement system. The image sharpness of the radiograph can be evaluated from the collimator ratio L/D, where L is the distance between the X-ray generator and the I.I., and D is the beam diameter. Image blurring decreases with increasing L/D. In this study, L/D was set at 225, and the image blur was estimated as 530 μm. Therefore, the void fraction in the vicinity of the tube surface is not discussed in this paper.

The uncertainty of the void-fraction measurement was evaluated in a pilot study using acrylic containers, with several containers of various sizes used to obtain known void fractions. The results are shown in Fig. 4., where α is the measured void fraction using X-ray radiography and α_{ref} is the reference void fraction obtained from the container's size. The resulting measurement uncertainty obtained was approximately ±5% in the absolute void fraction.

It has been reported that the average void-fraction profiles along the flow directions do not change significantly except at the outlet of the bundle (Dowlati et al. 1990). Further, Iwaki et al. (2004) measured the velocity fields in single-phase flow in both in-line and staggered tube bundles using a PIV and showed that the velocity components have no significant difference after the first row. Thus, in this study, evaluation of the void fraction was carried out around the fourth row for the in-line tube bundle and the third row for the staggered tube bundle.

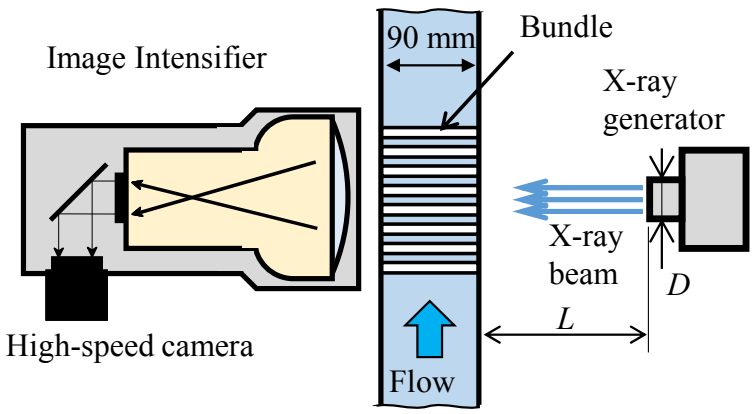

Fig. 3. The X-ray radiography measurement system.

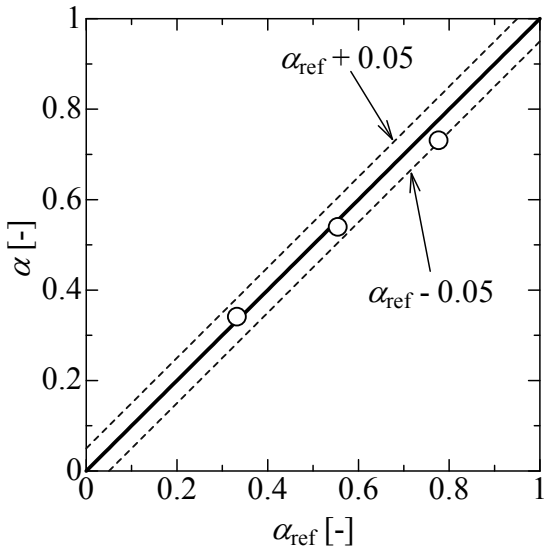

Fig. 4. Evaluation of the uncertainty of the void-fraction measurement.

2.3. Heat-transfer measurement around a tube

The schematic diagram of the measurement system is shown in Fig. 5. Heat transfer was evaluated using an electrode made of platinum wire with diameter 0.1 mm and length 30 mm placed in the center of the tube. The platinum wire was connected to a DC power supply to heat up the wire. The heat input, Q, can be obtained using the difference of the electrical voltage, V, at the platinum wire and the current, I, obtained using a reference resistance. It is well known that the resistance of platinum is proportional to temperature. Thus, the local heat-transfer coefficient, h, can be determined as follows:

$$h = \frac{Q}{A_{\mathrm{Pt}}(T_{\mathrm{Pt}} - T_f)} = \frac{IV}{A_{\mathrm{Pt}}(T_{\mathrm{Pt}} - T_f)} \qquad (5)$$

where A_{Pt} is the heat transfer area, T_{Pt} is the temperature of the platinum wire, and T_f is the fluid temperature measured at the test section. The heat-transfer coefficients around each tube were measured by rotating the tube every 15° at the center position of the fourth row for in-line and the third row for staggered, as shown in Fig. 2. The measurement results were averaged over 30 s.

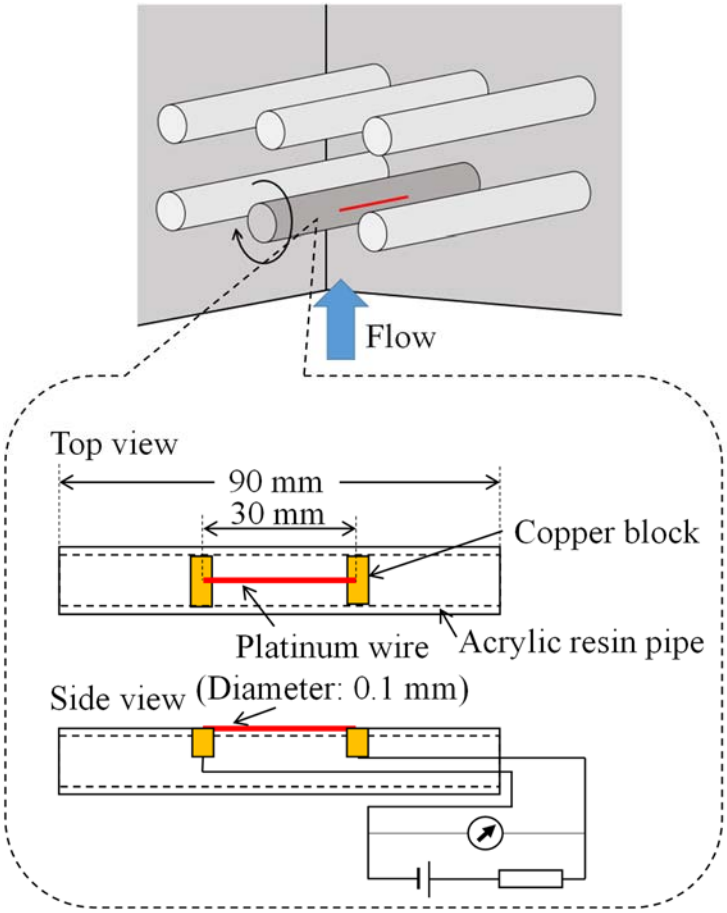

Fig. 5. Measurement system for heat transfer coefficient around a tube.

3. Results and discussion

3.1. Flow regime map

Examples of the obtained flow pictures for both tube bundles are shown in Fig. 6. Bubbly and intermittent flows were observed under the experimental conditions. In the bubbly flow, many bubbles with diameter less than the bundle gap flowed in the vertical gaps, and some bubbles passed through the bottom of the tubes in the in-line bundle. In intermittent flow, large bubbles with diameter three to four times greater than that of the bundle gap flowed intermittently. Following synchronization with the large diameter bubbles, reverse flow was confirmed around the near-wall bundle region.

Two-phase flow regime maps were constructed from the visual observation for both in-line and staggered tube bundles, shown in Fig. 7. For the in-line tube bundle, the bubbly flow was observed at lower J_G, and the flow regime changed to intermittent flow with increasing gas flow rate. The results are in good agreement with the flow regime map proposed by Noghrehkar et al. (1999). For the staggered

tube bundle, the bubbly flow regime slightly expanded to a higher J_G than that in the in-line tube bundle. The transition from bubbly to intermittent flow occurred at a lower J_G than that presented in the literature (Noghrehkar et al., 1999). The difference in the channel size and inlet conditions might have affected the transition of the flow regime.

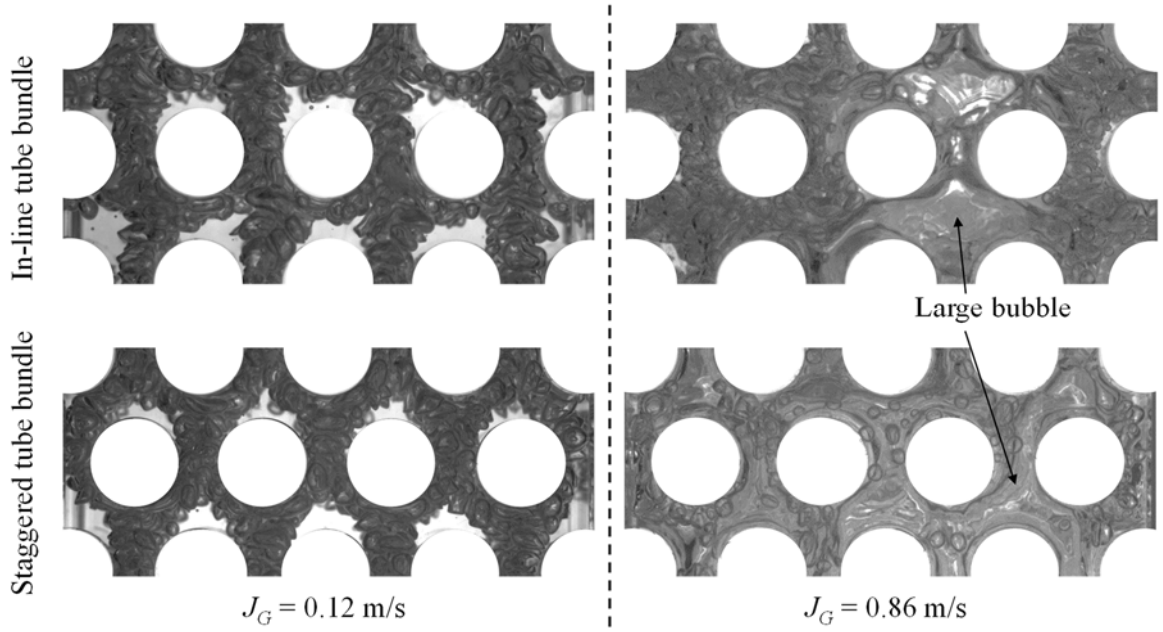

Fig. 6. Visualizations of the flow in the tube bundles.

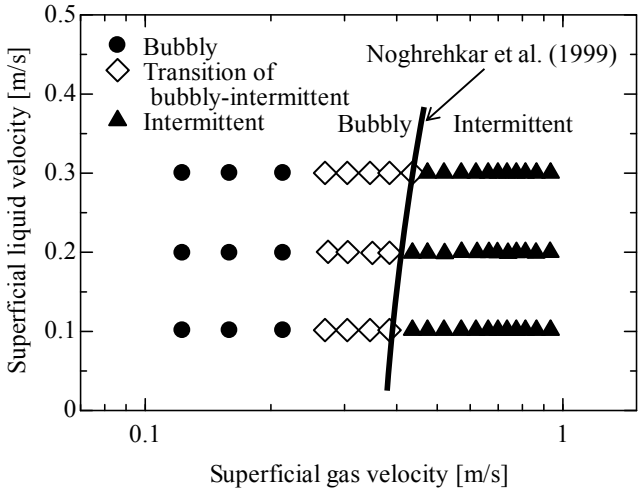

(a) In-line tube bundle

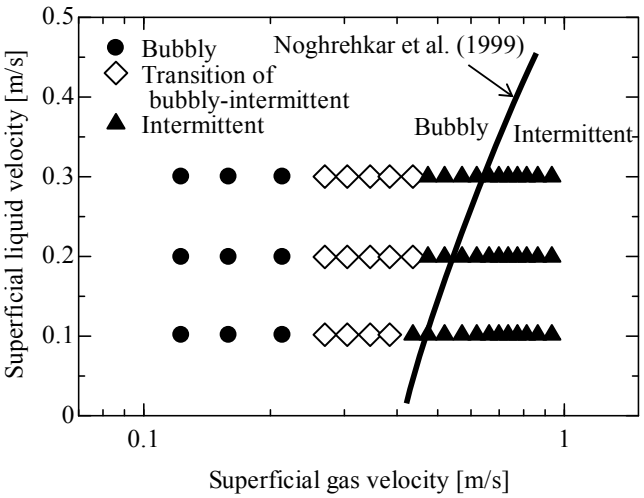

(b) Staggered tube bundle

Fig. 7. Flow regime map for the tube bundles.

3.2. Two-dimensional void-fraction distribution

The results of two-dimensional void-fraction distribution at G = 200 kg/(m^{2}s) (J_L = 0.2 m/s) are shown in Fig. 8. The measurement area was around the center tube in the fourth row from the inlet of the bundles. The definition of the area in the maximum and minimum gaps for the in-line tube bundle is shown in Fig. 2.

For the in-line tube bundle, many bubbles traveled along the vertical tube gaps, and the void

fraction became higher than that in the other region in bubbly flow. Some bubbles passed through the bottom of the tubes. As a result, the void fraction around the lower section of each tube became higher than that around the upper section of the tubes. The void fraction at the horizontal minimum gap was slightly higher than that at the maximum gap. With increasing gas flow rate, the void fraction gradually increased. In the transition between bubbly and intermittent flow, the void fraction distributions became almost flat in the tube bundle. The difference in the void fraction between the maximum and minimum gaps is small under the condition. In the intermittent flow regime, large bubbles intermittently passed through the tubes. As a result, the void fraction around the maximum gap and the vertical minimum gap increased. The maximum void fraction around the maximum gap and the horizontal minimum gap were almost the same. In contrast, the void fraction around the vertical minimum gap was slightly lower than that around the maximum and horizontal minimum gaps. Large bubbles intermittently passed between the tube gaps, and occupied the maximum and vertical minimum gaps. Consequently, a slightly lower void fraction was observed at the horizontal minimum gap.

For the staggered tube bundle, the fluctuation of bubbles movement with time was smaller than that in the in-line tube bundle in bubbly flow. The void fraction around the bottom of the tubes was slightly high in comparison to the horizontal tube side. Small bubbles traveled through the tube gaps and were distributed on both sides of the tubes at the bottom. Hence, the region where the void fraction is almost zero is clearly confirmed downstream of the tubes. The void-fraction distributions become almost flat in the tube bundle under the transition condition. The tendency of the void-fraction distribution is almost the same as that in the in-line tube bundle; however, the void fraction around the bottom of the tubes are slightly higher than that in the other region. At intermittent flow, the void fraction around the bottom of the tubes became much higher than the other region—which confirms that large bubbles tend to be stagnant around the bottom of tubes. As a result, the void fraction has a large distribution in comparison to that in the in-line tube bundle. Furthermore, the maximum void fraction in the staggered tube bundle was higher than that in the in-line tube bundle.

For the other conditions of G = 100 and 300 kg/(m^{2}s), the tendency of the void-fraction distributions were almost the same as that of G = 200 kg/(m^{2}s). This indicates that the distributions are dependent on the flow regimes.

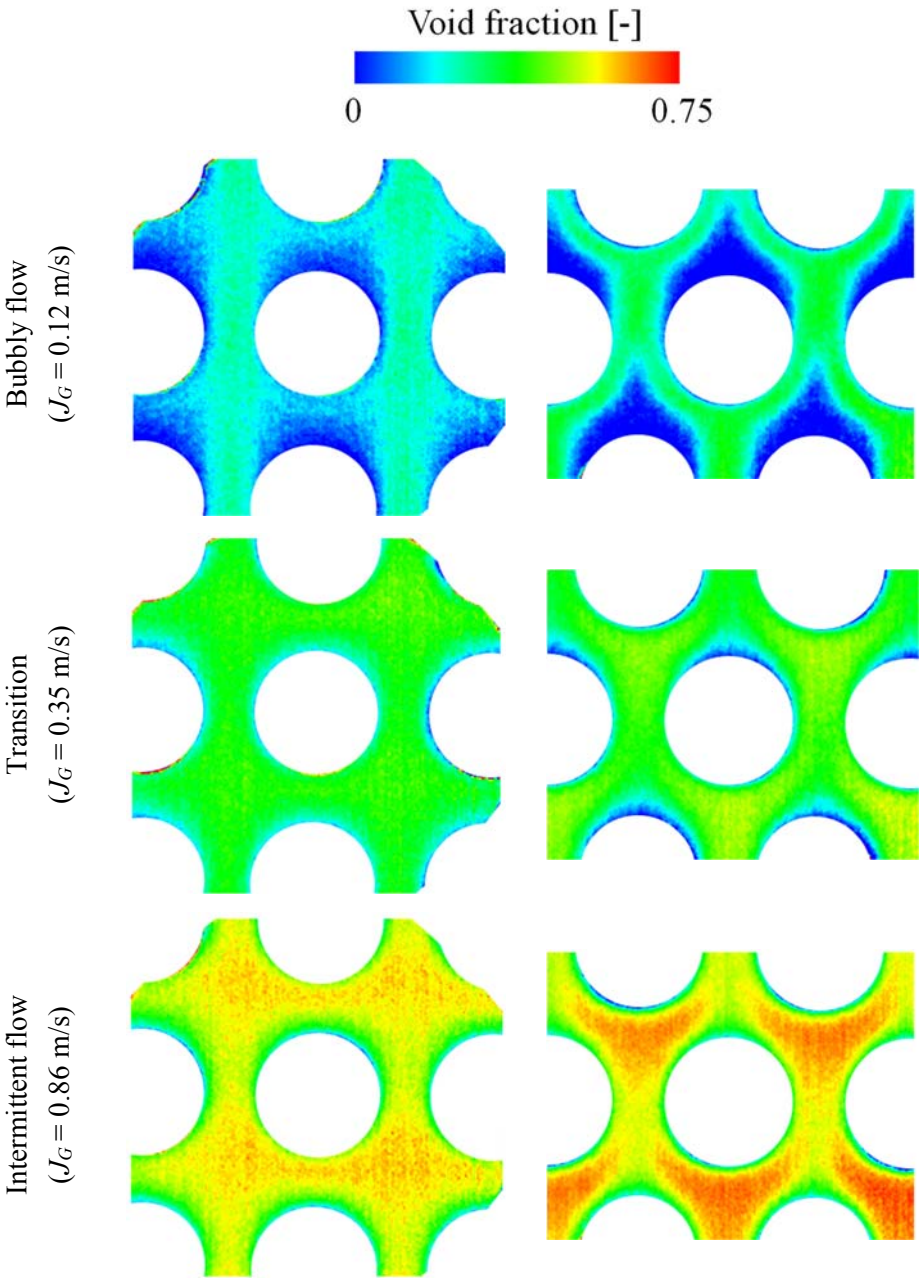

Fig. 8. Two-dimensional void fraction distributions (G = 200 kg/(m^{2}s)).

3.3. Average void fraction

Void fraction α can be expressed by the following expression:

$$\alpha = \left(1 + S\frac{\rho_G}{\rho_L}\left(\frac{1}{x} - 1\right)\right)^{-1} \quad (6)$$

where x is the quality and S is the velocity ratio of the gas and liquid phase, *i.e.*, $S = U_G/U_L$. Feenstra et al. (2000) proposed the following equation for predicting S in tube bundles considering the geometric parameter p/d:

$$S = 1 + 25.7\left(Ri \times Cap\right)^{0.5}\left(p/d\right)^{-1} \quad (7)$$

In this model, Richardson number R_i, and capillary number Cap are expressed as in the following equations:

$$Ri = \left(\rho_L - \rho_G\right)^2 ga / G \quad (8)$$

$$Cap = \eta_L U_G / \sigma \quad (9)$$

$$U_G = \frac{xG}{\alpha\rho_G} \quad (10)$$

where a is the gap between the tubes, η_L is the absolute viscosity of the liquid phase and σ is the surface tension. They developed the model based on their experimental data (Feenstra et al., 1995) and compared the equations with those in the literature for in-line and staggered tube bundles with p/d = 1.3−1.75.

The average void fractions between the third and fourth row were calculated in each bundle and condition from the two-dimensional void-fraction distributions. The results obtained were then compared with Eqns. (6) and (7), as shown in Fig. 9. The void fraction distributes between the homogeneous flow model and the maximum slip model (Chisholm, 1983). Although Feenstra's equation overestimated the void fraction in the in-line tube bundle, particularly for a lower mass flux of G = 100 and 200 kg/(m^{2}s), the equation could roughly predict the void fraction. In this study, the average void fraction in a cross-section was evaluated. Thus, the corner effect in the duct appears three-dimensionally. On the other hand, the chordal-average void fraction between the tubes was evaluated in other studies using γ-densitometers with beam sizes of 12.7 mm × 50.8 mm for Feenstra et al. (1995) and 24 mm × 50.8 mm for Dowlati et al. (1990). The differences in the evaluation area might affect the void fraction differences. Experimental results show that the void fractions for the staggered tube bundle are higher than that for the in-line tube bundle. The difference in the void fraction in-between the staggered and in-line bundles is approximately 20 %.

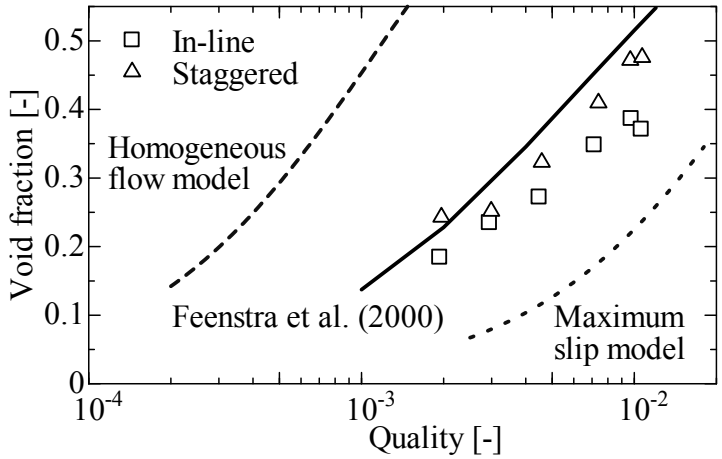

(a) G = 100 kg/(m^{2}s) (J_L = 0.1 m/s)

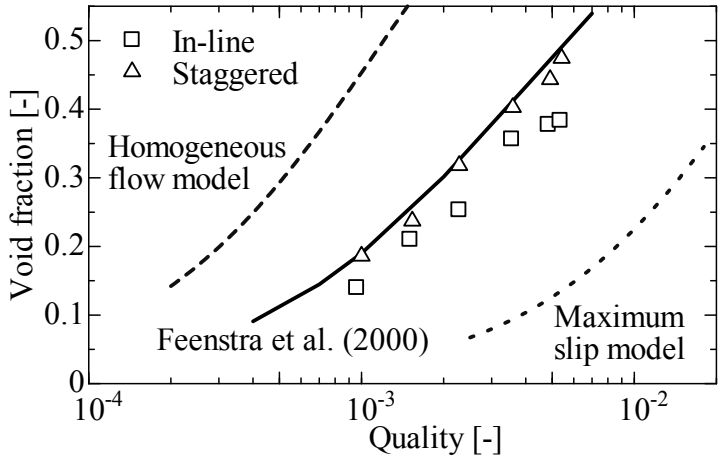

(b) G = 200 kg/(m^{2}s) (J_L = 0.2 m/s)

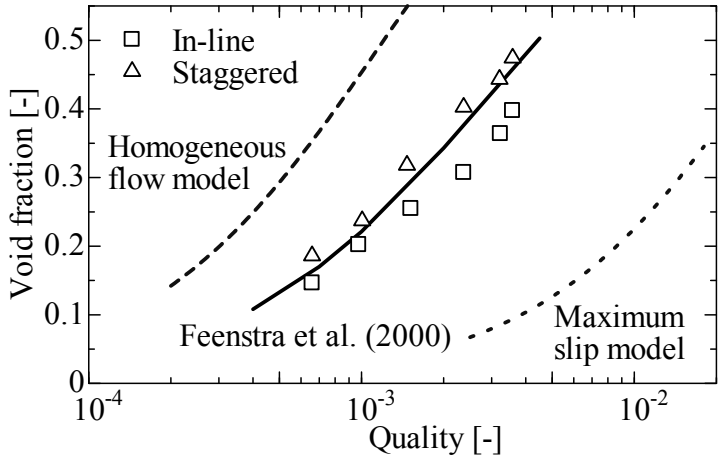

(c) G = 300 kg/(m^{2}s) (J_L = 0.3 m/s)

Fig. 9. Comparison of space-average void-fraction with in-line and staggered tube bundles.

3.4. Heat transfer around a tube

Fig. 10 depicts the heat-transfer coefficient around a tube at J_L = 0.2 m/s. The vertical axis indicates the local heat-transfer coefficients normalized by the average heat-transfer coefficient over the tube in single-phase flow for the in-line tube bundle. The value 0° represents the bottom of the tube, and the counterclockwise rotation is defined as positive degree.

For the in-line tube bundle, the heat-transfer coefficient under liquid single-phase flow increases from 0° and reaches the maximum value near ± 90°; thereafter, it takes minimum values around ± 135°. For the bubbly flow condition, the heat-transfer coefficient between ± 90 and 180° is higher than that in single-phase flow. With increased gas flow rate, the local heat transfer increases over the tube. Under the intermittent flow condition, distribution of the heat-transfer coefficient is confirmed to flatten over the tube, in comparison to that in single-phase flow. Because the void fraction around the tube is almost uniformly distributed, enhancement of the heat transfer occurred by bubbles motion all over the tube under the condition. This effect is confirmed around θ = ± 90–180°.

For the staggered tube bundle, the heat-transfer coefficient under the liquid single-phase condition peaks around ± 30° and bottoms around ± 120°. The average heat transfer around the tube is higher than that for the in-line tube in single-phase flow. In the bubbly flow condition, it can be said that the bubbles motion slightly enhances the heat transfer mainly downstream of the tube. However, the distribution still takes the maximum value around ± 30°, and it is similar to that in single-phase flow. Therefore, the agitation effect for increasing the heat transfer is less than that for the in-line tube bundle. In the intermittent flow condition, the heat-transfer coefficient around the downstream of the tube becomes higher owing to the bubbles motion. The values around ± 90° were slightly higher than that at the other positions.

Fig. 11 compares the average heat-transfer coefficient over the tube for in-line and staggered tube bundles. The heat transfers were normalized by the average heat transfer in single-phase flow at J_L = 0.2 m/s in in-line tube bundle. The heat-transfer coefficient in single-phase flow increases with J_L. In the bubbly flow condition, although the bubbles motion increased the local heat transfer for the in-line tube bundle more than that for the staggered tube bundle, the average heat transfer in the staggered tube bundle is slightly higher than that in the in-line tube bundle. However, in the intermittent flow condition, the average heat transfer became higher in the in-line tube bundle than that in the staggered tube bundle.

This is because bubbles motion more effectively increased the heat transfer, particularly around $\theta = \pm$ 90–180°, for the in-line bundle than that in the staggered. The average heat-transfer coefficient in the intermittent flow increased to more than 1.5 times that in the single-phase flow.

The average void fraction does not directly represent the liquid turbulence and agitation. Therefore, enhancement in heat transfer is not proportional to the local void fraction. However, the relation between the local void fraction and heat transfer was obviously confirmed from the experimental results. Enhancement in the heat transfer by bubbles motion was apparent where the local heat transfer in single-phase flow was relatively low. Furthermore, the enhancement was also confirmed where the local void fraction was relatively low. Thus, it can be said that bubbles motion agitated the liquid phase, resulting in improved heat transfer. Although increases in the heat-transfer coefficient by bubbles motion was confirmed for both the in-line and staggered tube bundles, the effect was more apparent for the in-line array than for the staggered array. The relative velocity between the gas and liquid is larger for the in-line bundle than for the staggered bundle at the same J_G and J_L because the average void fraction is lower for the in-line bundle. Therefore, the effect of liquid agitation was more apparent for the in-line bundle. However, as the heat transfer for the staggered tube bundle in single-phase flow was higher than that for the in-line tube bundle, better results for average heat-transfer coefficients for the staggered tube bundle were obtained in the bubbly flow condition, whereas the tendency was opposite in the intermittent flow condition. Therefore, the staggered tube bundle is suitable for bubbly flow conditions, whereas the in-line tube bundle is better for intermittent flow conditions.

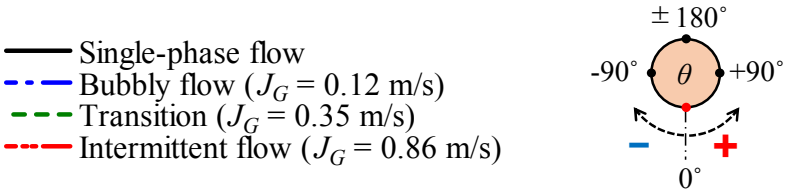

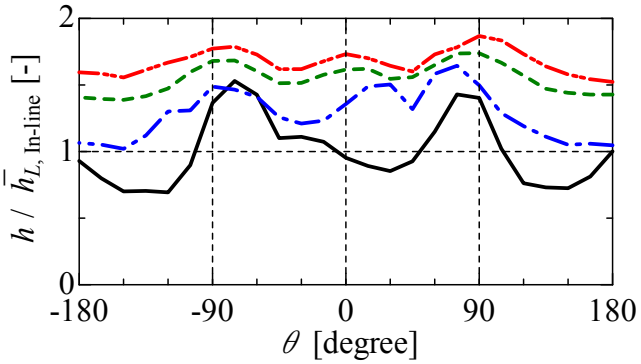

(a) In-line tube bundle

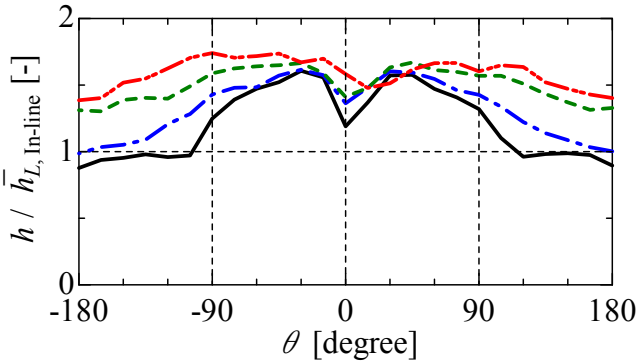

(b) Staggered tube bundle

Fig. 10. Heat transfer coefficient around a tube (J_L = 0.2 m/s)

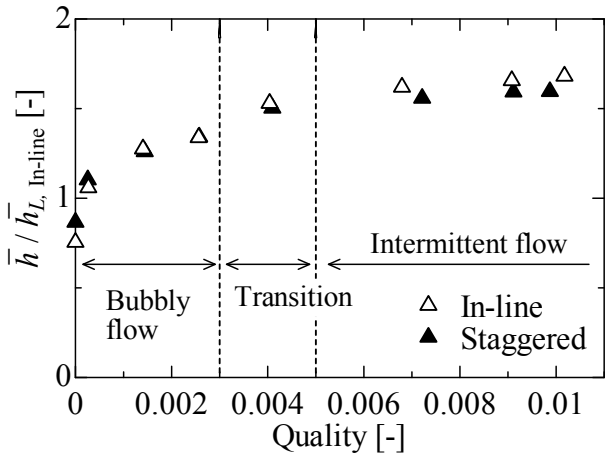

(a) G = 100 kg/(m^{2}s) (J_L = 0.1 m/s)

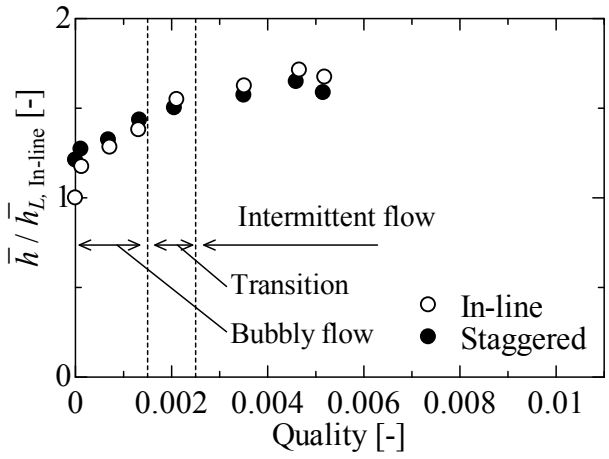

(b) G = 200 kg/(m^{2}s) (J_L = 0.2 m/s)

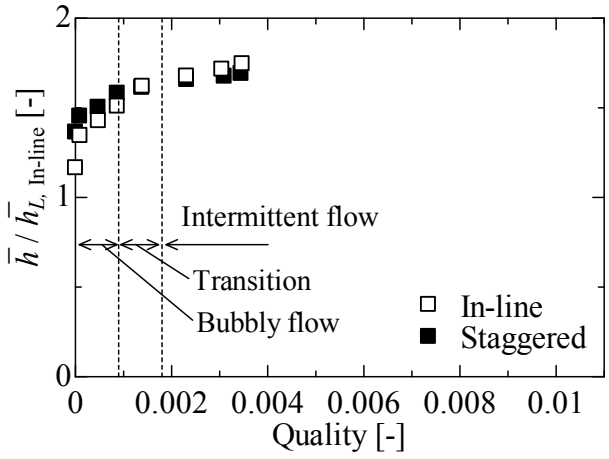

(c) G = 300 kg/(m^{2}s) (J_L = 0.3 m/s)

Fig. 11. Comparison of average heat-transfer coefficient around a tube for in-line and staggered tube bundles.

4. Conclusions

In this study, to clarify the effect of tube arrays on void fraction and heat-transfer characteristics, two-dimensional void-fraction distribution and heat-transfer coefficient were compared for in-line and staggered tube bundles under bubbly to intermittent flow conditions. The tube bundles contained eight rows with five 15-mm outer-diameter tubes in each row. The two-dimensional void-fraction distributions were obtained using X-ray radiography, and the heat-transfer coefficients around each tube were measured using a platinum wire placed on the tube. For rotating the tube, the relation between the local void fraction and heat transfer was discussed. The main results are summarized as follows:

The time-average void fraction increased at the maximum and vertical minimum gaps for the in-line tube bundle, whereas the void fraction increased upstream of the tubes for the staggered tube bundle. The average void fraction for the staggered tube bundle was approximately 20% higher than that for the in-line tube bundle.

Bubbles motion agitated the liquid phase, resulting in improved heat transfer in the bubbly to intermittent flow conditions. The effect was more apparent for the in-line bundle at $\theta = \pm$ 90–180°.

As the heat transfer for the staggered tube bundle in single-phase flow was higher than that for the in-line tube bundle, better results were obtained for the average heat-transfer coefficients of the staggered tube bundle in the bubbly flow condition. However, the average heat transfer for the in-line bundle was better in the intermittent flow condition. Thus, an array of staggered bundles for upstream regions and in-line bundles for downstream regions is suitable for heat exchangers.

References

Aprin, L., Mercier, P., Tadrist, L., 2007. Experimental analysis of local void fractions measurements for boiling hydrocarbons in complex geometry. Int. J. Multiphase Flow 33, 371−393.

Aprin, L., Mercier, P., Tadrist, L., 2011. Local heat transfer analysis for boiling of hydrocarbons in complex geometries: A new approach for heat transfer prediction in staggered tube bundle. Int. J. Heat and Mass Transfer 54, 4203−4219.

Burnside, B.M., Miller, K.M., McNeil, D.A., Bruce, T., 2001. Heat transfer coefficient distributions in an experimental kettle reboiler thin slice. Chem. Engin. Research and Des. 79, 445–452.

Chan, A.M.C., Shoukri, M., 1987. Boiling characteristics of small multitube bundles. J. Heat Transfer 109, 753−760.

Chisholm, D., 1983. Two-phase flow in pipelines and heat exchangers, George Godwin, London and New York.

Dowlati, R., Kawaji, M., Chan, A.M.C., 1990. Picth-to-diameter effect on two-phase flow across an in-line tube bundle. AIChE J. 36, 765−772.

Dowlati, R., Chan, A.M.C., Kawaji, M., 1992. Hydrodynamics of two-phase flow across horizontal in-line and staggered rod bundle, Trans. ASME 114, 450−456.

Dowlati, R., Kawaji, M., Chan, A.M.C., 1996. Two-phase crossflow and boiling heat transfer in horizontal tube bundles, Tran. ASME 118, 124−131.

Feenstra, P.A., Judd, R.L., Weaver, D.S., 1995. Fluidelatic instability in a tube array subjected to two-phase R-11 cross-flow, J. Fluids and Structures 9, 747−771.

Feenstra, P.A., Weaver, D.S., Judd, R.L., 2000. An improved void fraction model for two-phase cross-flow in horizontal tube bundles. Int. J. Multiphase Flow 26, 1851−1873.

Iwaki, C., Cheng, K.H., Monji, H., Matsui, G., 2004. PIV measurement of the vertical cross-flow structure over tube bundles. Exp. in Fluids 37, 350−363.

Iwaki, C., Cheong, K.H., Monji, H., Matsui, G., 2005. Vertical, bubbly, cross-flow characteristics over tube bundles. Exp. in Fluids 39, 1024−1039.

Karas, M., Zajac, D., Ulbrich, R., 2014. Experimental investigation of heat transfer performance coefficient in tube bundle of shell and tube heat exchanger in two-phase flow. Archives of Thermodynamics 35, 87−98.

Kondo, M., Nakajima, K., 1980. Experimental investigation of air-water two phase upflow across horizontal tube bundles (Part I Flow pattern and void fraction). Bulletin of the JSME 23, 385−393.

McNeil, D.A., Sadikin, A.， Bamardouf, K.H., 2012. A mechanistic analysis of shell-side two-phase flow in an idealised in-line tube bundle, Int. J. Multiphase Flow 45, 53−69.

Noghrehkarm, G.R., Kawaji, M., Chan, A.M.C., 1999. Investigation of two-phase flow regimes in tube bundles under cross-flow conditions, Int. J. Multiphase Flow 25, 857−874.

Ulbrich R., Mewes, D., 1994. Vertical, upward gas-liquid two-phase flow across a tube bundle. Int. J. Multiphase Flow 20, 249−272.

Xu, G.P., Tso, C.P., Tou, K.W., 1998. Hydrodynamic of two-phase in vertical up and down-flow across a horizontal tube bundle. Int. J. Multiphase Flow 24, 1317−1342.